

## INTERSTELLAR PLASMA WEATHER EFFECTS IN LONG-TERM MULTI-FREQUENCY TIMING OF PULSAR B1937+21

R. RAMACHANDRAN, P. DEMOREST, D. C. BACKER

Department of Astronomy and Radio Astronomy Laboratory, University of California, Berkeley, CA 94720-3411, USA;  
 e-mail: ramach, demorest, dbacker@astro.berkeley.edu

I. COGNARD

Laboratoire de Physique et Chimie de l'Environnement, CNRS, 3A avenue de la Recherche Scientifique, F-45071 Orleans, France

A. LOMMEN

Department of Physics and Astronomy, Franklin and Marshall College, P.O.Box 3003, Lancaster, PA 17604, USA  
*Draft version October 7, 2018*

### ABSTRACT

We report here on variable propagation effects in over twenty years of multi-frequency timing analysis of pulsar PSR B1937+21 that determine small-scale properties of the intervening plasma as it drifts through the sight line. The phase structure function derived from the dispersion measure variations is in remarkable agreement with that expected from the Kolmogorov spectrum, with a power law index of  $3.66 \pm 0.04$ , valid over an inferred scale range of 0.2–50 A.U. The observed flux variation time scale and the modulation index, along with their frequency dependence, are discrepant with the values expected from a Kolmogorov spectrum with infinitesimally small inner scale cutoff, suggesting a caustic-dominated regime of interstellar optics. This implies an inner scale cutoff to the spectrum of  $\sim 1.3 \times 10^9$  meters. Our timing solutions indicate a transverse velocity of 9 km sec<sup>-1</sup> with respect to the solar system barycenter, and 80 km sec<sup>-1</sup> with respect to the pulsar's LSR. We interpret the frequency dependent variations of DM as a result of the apparent angular broadening of the source, which is a sensitive function of frequency ( $\propto \nu^{-2.2}$ ). The error introduced by this in timing this pulsar is  $\sim 2.2 \mu\text{s}$  at 1 GHz. The timing error introduced by “image wandering” from the slow, nominally refractive scintillation effects is about 125 nanosec at 1 GHz. The error accumulated due to positional error (due to image wandering) in solar system barycentric corrections is about 85 nanosec at 1 GHz.

*Subject headings:* ISM: general — pulsars: general — radio continuum: general — scattering — turbulence

### 1. INTRODUCTION

The dispersion measure (DM) of a pulsar probes the column density of free electrons along the line of sight (LOS). Observed DM variations over time scales of several weeks to years sample structures in the electron plasma over length scales of  $10^{10}$  m to  $10^{12}$  m. Diffraction of pulsar signals is the result of scattering by structures on scales below the Fresnel radius,  $10^8$  m or so. The DM as well as the scattering measure (SM) variability along the LOS to the Crab pulsar was first reported by Rankin & Isaacman (1977), who reported that the DM variability poorly correlated with the SM variability. Helfand et al. (1980) inferred an upper limit for DM variations of a few parts in a thousand for several pulsars. In an earlier study of PSR B1937+21 Cordes et al. (1990) measured a DM change of  $\Delta DM \sim 0.003 \text{ pc cm}^{-3}$  over a period of a thousand days. The work of Phillips & Wolszczan (1991) presented the variations of DM observed along the LOS to a few pulsars. They connected these variations to those on diffractive scales, and derived an electron density fluctuation spectrum slope of  $3.85 \pm 0.04$  over a scale range of  $10^7 - 10^{13}$  meters. Backer et al. (1993) report on further DM variability and show that the amplitude of the variations known at that time are consistent with a scaling by the square root of DM. Another important investigation by Kaspi et al. (1994) studied DM variations of the millisecond pulsars PSR B1937+21 and B1855+09 over a time interval of calendar years 1984 to 1993. In addition to establishing a secular variation in DM over this time interval, they also show that the underlying den-

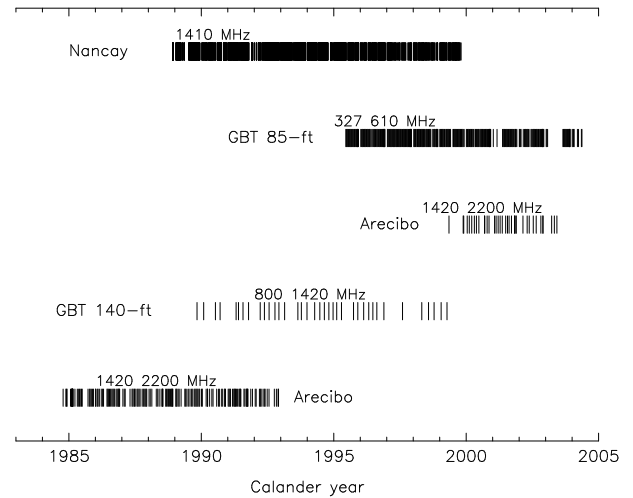


FIG. 1.— Summary of our data sample. See text for details.

sity power spectrum has an index of  $3.874 \pm 0.011$ , which is close to what we would expect if the density fluctuations are described by Kolmogorov spectrum. An anomalous dispersion event towards the Crab pulsar was reported by Backer et al. (2000), where they report a DM “jump” as large as  $0.1 \text{ pc cm}^{-3}$ .

TABLE 1  
TEMPLATE FIT PARAMETERS AT VARIOUS FREQUENCIES.

$\nu$ (MHz)	backend	$w_1$	$l_2$	$w_2$	$h_2$	$l_3$	$w_3$	$h_3$
327	GBPP	8.7	0	0	0	186.9	12.0	0.51
430	ABPP	10.3	7.0	2.5	0.19	186.8	12.4	0.53
610	GBPP	9.4	7.1	2.9	0.34	187.3	10.8	0.60
863	EBPP	8.9	7.7	5.2	0.38	187.7	10.9	0.55
1000	GBPP	9.2	8.6	3.9	0.56	187.9	11.3	0.54
1419	ABPP	8.5	8.5	3.7	0.37	187.5	10.1	0.45
1689	EBPP	9.1	9.2	3.9	0.37	187.4	10.5	0.40
2200	GBPP	9.4	9.8	3.2	0.29	187.6	10.4	0.36
2379	ABPP	10.0	9.8	3.0	0.29	187.1	10.8	0.33

In this work, we present results of various long term monitoring programs on PSR B1937+21. Our data, which includes that of Kaspi, Taylor & Ryba (1994), spans calendar years from 1983 to 2004. These data sets have been taken with five different telescopes, the NRAO<sup>1</sup> Green Bank 42-m (140-ft) and 26-m (85-ft) telescopes, the NAIC<sup>2</sup> Arecibo telescope and the Nançay telescope, at frequency bands of 327, 610, 800, 1400 and 2200 MHz. After giving the details of our observations in §2, we describe our analysis methods in §3. This is followed in §4 by a discussion on the distribution of scattering material along the LOS. As we describe, the knowledge of temporal and angular broadening of the source, proper motion, and scintillation based velocity estimates enables us to at least qualitatively study the distribution of scattering matter as well as properties of its wave-number spectrum.

We have measured some of the basic refractive scintillation parameters from our observations, and these are discussed in §5. The frequency dependence of the refractive scintillation time scale and the modulation index indicate a caustic-dominated regime that results from a large inner scale in the spectrum.

We have detected DM variations as a function of time and frequency. We determine the phase structure function of the medium with the knowledge of the time dependent DM variations, which is consistent with a Kolmogorov distribution of density fluctuations between scale sizes of about 1 to 100 A.U. These are summarized in §6 and §7.

PSR B1937+21 is known for its short term timing stability. However, the achievable long term timing accuracy is suspected to be seriously limited by the interstellar scattering properties. With our sensitive measurements, we are in a position to quantify these errors. In §8, we describe in detail various sources of these errors and quantify them.

## 2. OBSERVATIONS

We have used five different primary data sets for this analysis. The first set is the 1984–1992 Arecibo pulse timing and dispersion measurements obtained by Kaspi et al. (1994; hereafter KTR94). Their observations were performed with their Mark II backend (Rawley 1986; Rawley, Taylor & Davis 1988) and later their Mark III backend (Stinebring et al. 1992) at two different radio frequency bands, 1420 MHz and 2200 MHz. Their analysis methods are described in KTR94.

<sup>1</sup> The National Radio Astronomy Observatory (NRAO) is owned and operated by Associated Universities, Inc under contract with the US National Science Foundation.

<sup>2</sup> The National Astronomy and Ionosphere Center is operated by Cornell University under contract with the US National Science Foundation.

TABLE 2  
PARAMETERS OF PSR B1937+21.

Parameter	value
PSR	1937+21
RAJ (hh:mm:ss)	19:39:38.561 (1)
DECJ (dd:mm:ss)	21:34:59.136 (6)
PMRA (mas yr <sup>-1</sup> )	0.04 (20)
PMDEC (mas yr <sup>-1</sup> )	-0.45 (6)
$f$ (Hz)	641.9282626021 (1)
$\dot{f}_{-15}$ (Hz s <sup>-1</sup> )	-43.3170 (6)
$\ddot{f}_{-26}$ (Hz s <sup>-2</sup> )	1.5 (3)
PEPOCH (MJD)	47500.000000
START	45985.943
FINISH	52795.286
EPHEM	DE405
CLK	UTC (NIST)

The second data set is from 800-MHz and 1400-MHz observations at the NRAO 140-ft telescope in Green Bank, WV. The Spectral Processor backend, a hardware FFT device, was used. Details about the observations and analysis are contained in an earlier report on dispersion measure variability (Backer et al. 1993).

The third data set consists of observations at 327 MHz and 610 MHz using the 26m (85-ft) pulsar monitoring telescope at NRAO’s Green Bank, WV site. Room temperature (uncooled) receivers at the two bands are mounted off-axis. At 327 MHz the total bandwidth used was 5.5 MHz, and 16 MHz was used at 610 MHz. The two orthogonally polarized signals were split into 32 frequency channels in a hybrid analog/digital filter bank in the GBPP (Green Bank–Berkeley Pulsar Processor). Dispersion effects were removed in the GBPP in real-time with a coherent (voltage) deconvolution algorithm. At the end of the real-time processing folded pulse profiles were recorded for each frequency channel and polarization. Further details of the backend and analysis can be found in Backer, Wong & Valanju (2000). PSR B1937+21 was observed for about two hours per day starting in mid-1995.

The fourth data set comes from a bi-monthly precision timing program that includes B1937+21 at the Arecibo Observatory which we started in 1999 after the telescope upgrade. Signals at 1420 MHz and 2200 MHz were recorded using the ABPP backend (Arecibo–Berkeley Pulsar Processor), which is identical to the GBPP. Our typical observing sessions at 1420 MHz and 2200 MHz had bandwidths of 45 MHz and 56 MHz, respectively, and integration times of approximately 10 minutes per session.

The fifth data set is from a pulsar timing program that has been ongoing since 1989 October with the large decimetric radio telescope located at Nançay, France. The Nançay telescope has a surface area of 7000 m<sup>2</sup>, which provides a telescope gain of 1.6 K Jy<sup>-1</sup>. Observations are performed with dual-linear feeds at frequencies 1280, 1680 and 1700 MHz. Then the signal is dedispersed by using a swept frequency oscillator (at 80 MHz) in the receiver IF chain. The pulse spectra are produced by a digital autocorrelator with a frequency resolution of 6.25 kHz. Cognard et al. (1995) describe in detail the backend setup and the analysis procedure.

A small amount of additional data from the Effelsberg telescope was used in our profile analysis. At Effelsberg the

EBPP backend, a copy of the GBPP/ABPP, was used.

### 3. BASIC ANALYSIS

We first present several results from the analysis of these data sets: a description of the frequency-dependent profile template used for timing; spin and astrometric timing parameters from high frequency data; pulse broadening, flux densities and dispersion measure as functions of time. In §4 we proceed to interpret these results and return to finer details regarding dispersion measure variations in §6.

Our basic data set consists of average pulse profiles obtained approximately every 5 minutes in each of the radio frequency bands – 327, 610, 800, 1420 and 2200 MHz. Figure 1 provides a graphical summary of observation epochs vs date. For data sets corresponding to all frequencies except 327 MHz, *Times of Arrival* (TOAs) were computed by cross correlating these average profiles with a template profile. The template profile at a given frequency was made by using multiple Gaussian fits to very high signal to noise ratio average profiles at that frequency; the interactive program *bfit*, which is based on M. Kramer’s original program *fit* was used. These fit parameters are listed in Table 1. Col. 1 in the Table gives the radio frequency and the backend name is in col. 2. Col. 3 gives the width of component 1 ( $w_1$ ; its location is taken to be 0 degrees and its amplitude is set to 1.0); cols. 4-6 and cols. 7-9 give the location ( $l$ ), width ( $w$ ) and amplitude ( $h$ ) values for components 2 and 3, respectively. The location and width are given in units of longitudinal degrees, where  $360^\circ$  indicates one full rotation cycle. The results of this analysis can be compared with that of Foster et al. (1991) which are given on the line at 1000 MHz<sup>3</sup>. There is reasonable agreement for all values except  $h_2$  which must have been erroneously entered in Table 4 of Foster et al. In our analysis templates corresponding to arbitrary frequencies are produced by spline-interpolation of the component parameters.

We used the Arecibo (1420 MHz and 2200 MHz) TOAs, and the GBT 140-ft (800 MHz and 1420 MHz) TOAs to fit for pulsar spin (rotation frequency ( $f$ ), first time derivative ( $\dot{f}$ ), and second time derivative ( $\ddot{f}$ )) and astrometric (position (RAJ, DECJ), proper motion (PMRA,  $\mu_\alpha$ , along right ascension, and PMDEC,  $\mu_\delta$ , along declination) parameters. All TOAs were referred to the UTC time scale kept by the National Institute of Standards and Technology (NIST) via GPS satellite comparison. We removed the effects of variable dispersion from this fitting procedure with weekly estimation of DMs and subsequent extrapolation of the dual frequency data to infinite frequency prior to parameter estimation. The nature of achromatic timing noise makes it particularly difficult to determine a precise timing model. As one adds additional higher derivatives of rotation frequency (e.g., a third derivative), the best fit parameters change by amounts much larger than the nominal errors reported by the package that we used, TEMPO. The results are listed in Table 2. The errors presented in the table incorporates the range of variation of each parameter, as additional derivative terms are included. In comparison to Kaspi, Taylor & Ryba (1994), the derived proper motion values are marginally different. We attribute this difference to the variable influence of timing noise. An important point that needs to be stressed here is that there is no reason for us to assume that the higher derivative terms of rotation period (e.g.,  $\ddot{f}$  or higher) has anything to do with the radiative braking index. They are most likely dominated

<sup>3</sup> The widths  $w_1$  and  $w_3$  are inverted in Table 4 of Foster et al.

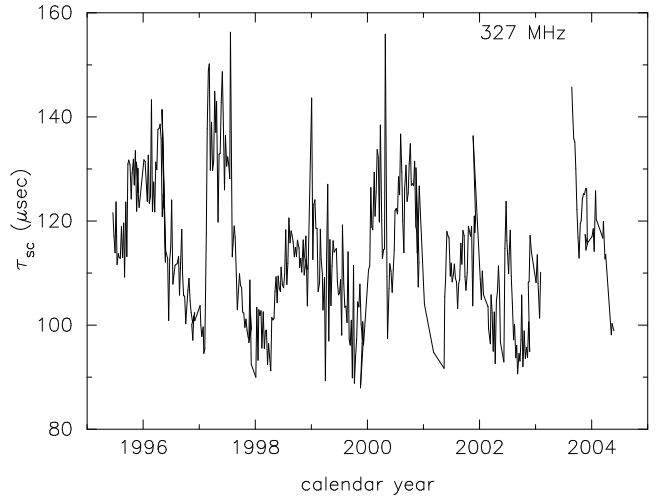


FIG. 2.— Measured temporal pulse broadening timescale ( $\tau_{sc}$ ) as a function of time at 327 MHz.

by some intrinsic instabilities of the star itself, or some other perturbation on the star.

Extension of dispersion measurement to 327 MHz requires removal of the time-variable broadening of the intrinsic pulse profile owing to multipath propagation in the interstellar medium. We deconvolved the effect of interstellar scattering following precepts first introduced by Rankin et al. (1970). We assume that the interstellar temporal broadening is quantified in terms of convolution of a Gaussian function and a truncated exponential function. If there is only one scattering screen along the LOS, the assumption of a truncated exponential function will suffice to represent the scatter broadening. However, since the scattering may arise from material distributed all along the LOS, a more realistic representation is approximated by a truncated exponential function “smoothed” (convolved) with a Gaussian function. The intrinsic pulse profile was estimated by extrapolation of parameters from the higher frequency profiles. In the deconvolution procedure, we minimized the normalized  $\chi^2$  value by varying the width of the Gaussian  $w_g$  and the decay time scale of the truncated exponential  $\tau_e$ , while keeping the intrinsic pulse profile fixed. The pulse scatter broadening is quantified as  $\tau_{sc} = (w_g^2 + \tau_e^2)^{1/2}$ . We repeated this for average profiles obtained at every epoch to obtain the  $\tau_{sc}$  measurement. In our fits, the average value of  $w_g$  came to about  $74 \mu\text{sec}$ , whereas the corresponding value for  $\tau_e$  was about  $85 \mu\text{sec}$ . The measurement of  $\tau_{sc}$  versus time at 327 MHz is plotted in the Figure 2. This quantity has a mean value of  $120 \mu\text{s}$ , an RMS variation of  $20 \mu\text{s}$ , and a fluctuation timescale of  $\sim 60$  days. We explain these variations as the result of refractive modulation of this inherently diffractive parameter in discussion below. The estimated RMS variation at the next higher frequency in our data set, 610 MHz, is  $\sim 2.5 \mu\text{s}$ , using a frequency dependence of  $\tau_{sc} \propto \nu^{-4.4}$ . This is too small to allow fitting at this frequency band.

In the strong scintillation regime, time dependent variations in the observed flux occur in two distinct regimes — *diffractive* and *refractive*. The diffractive effects are dominated by structures smaller than the Fresnel scale, and appear on short time scales and over narrow bandwidths. In our observations diffractive modulations are strongly suppressed. On the other

hand refractive effects occur on days time scales and are correlated over wide bandwidths. We have analyzed our best data sets – the densely sampled data at 327 MHz and 610 MHz from Green Bank and at 1410 MHz from Nançay – for flux density variations as a function of time. The data are presented in Figure 3.

In analyzing the low frequency flux data from Green Bank, we have not adopted a rigorous flux calibration procedure. While there is a pulsed calibration noise source installed in this system, equipment changes and the nature of the automated observing have led to large gaps in the calibration record. Rather than dealing with a mix of calibrated and uncalibrated data, or lose a large fraction of the data, we decided not to apply any calibration. Instead, we normalize our data by assuming the system temperature is constant. In order to see what effect this has on our results, we did two tests.

First, we analyzed observations of PSR B1641–45, taken with the same system, over a similar time range. This pulsar is known to have a very long refractive timescale,  $T_{\text{ref}} > 1800$  days (Kaspi & Stinebring, 1992), so it can be used as a flux calibrator. In our data, we find it to have a modulation index,  $m = 0.10$ . This immediately puts a upper limit of 10% on any systematic gain and/or system temperature variations. Since modulation adds in quadrature, and we observe modulation indices of  $m \sim 0.4$  for PSR B1937+21, gain fluctuations represent at most a small fraction of the observed modulation.

We also considered the possibility that gain variations could influence our measurement of  $T_{\text{ref}}$ . This might happen if they occur with a characteristic timescale longer than 1 day. In order to test this, we analyzed observations of the Crab pulsar, PSR B0531+21, again taken with the same system over the same time range. The refractive parameters of this pulsar were studied in detail by Rickett & Lyne (1990). It makes a good comparison since it has modulation index of  $m = 0.4$  at 610 MHz, very similar to PSR B1937+21. Applying the structure function analysis (see §5) to this data gives  $T_{\text{ref}} = 11$  days at 610 MHz, and  $T_{\text{ref}} = 63$  days at 327 MHz, consistent with the previously published results and a scaling law of  $T_{\text{ref}} \propto \nu^{-2.2}$ .

The procedure that we have adopted to calibrate our data set from Nançay telescope is described in detail in Cognard et al. (1995).

#### 4. DISTRIBUTION OF SCATTERING MATERIAL ALONG THE LINE OF SIGHT

Several authors have shown how the scattering parameters of a pulsar can be used to assess the distribution of scattering material along the LOS (Gwinn et al. 1993; Deshpande & Ramachandran 1998; Cordes & Rickett 1998). This results from the varied dependences of the scattering parameters on the fractional distance of scattering material along the LOS. PSR B1937+21 is viewed through the local spiral arm as well as the Sagittarius arm which are both potential sites of strong scattering. The parameters employed in this analysis are: the temporal pulse broadening by scattering ( $\tau_{\text{sc}}$ ); or its conjugate parameter  $\Delta\nu$ , the diffractive scintillation bandwidth), the diffractive scintillation time scale ( $T_{\text{diff}}$ ), the angular broadening from scattering ( $\theta_H$ ), the proper motion of the pulsar ( $\mu_\alpha, \mu_\delta$ ), and a distance estimate of the pulsar ( $D$ ).

Let us first compare  $\theta_H$  and  $\tau_{\text{sc}}$  that are the result of multiple scattering along the LOS, and express them as (Blandford & Narayan 1985)

$$\tau_{\text{sc}} = \frac{1}{2cD} \int_0^D x(D-x) \psi(x) dx \quad (1)$$

$$\theta_H^2 = \frac{4 \ln 2}{D^2} \int_0^D x^2 \psi(x) dx. \quad (2)$$

In these equations,  $x$  is the coordinate along the LOS, with the pulsar at  $x = 0$  and the observer at  $x = D$ .  $\psi(x)$  is the mean scattering rate. If the scattering material is uniformly distributed along the LOS, then the relation between the two quantities can be expressed as  $\theta_H^2 = 16 \ln 2 (c\tau_{\text{sc}}/D)$ . With the distance to the pulsar of 3.6 kpc to the pulsar (according to the distance model of Cordes & Lazio 2002), and the average pulse broadening time scale of 120  $\mu\text{s}$  (from the present work), we obtain an estimate of the angular broadening,  $\theta_\tau$ , of 12 mas. This is in modest agreement with the measured value of  $14.6 \pm 1.8$  mas (Gwinn et al. 1993), given the uncertainty in the distance to the pulsar and the simple assumption that the scattering material is uniformly distributed along the LOS.

Next, we formulate two approaches to estimation of the velocity of the LOS with respect to the scattering medium, and use these approaches to assess the location and extent of the medium. The transverse velocity of the pulsar based on the measured proper motion (Table 2) an assumed distance of  $D = 3.6$  kpc (Cordes & Lazio 2002) is 9  $\text{km s}^{-1}$ . This value is the velocity of the pulsar with respect to the solar system barycenter. With the assumed ‘‘Flat Rotation Curve’’ linear velocity of the Galaxy of 225  $\text{km s}^{-1}$ , and the Sun’s peculiar velocity of 15.6  $\text{km s}^{-1}$  in the Galactic coordinate direction of  $(l, b) = (48.8^\circ, 26.3^\circ)$  (Murray 1986), the transverse velocity of the pulsar in its LSR ( $V_p$ ) is 80  $\text{km s}^{-1}$ .

The *scintillation velocity* ( $V_{\text{iss}}$ ), which is an estimate of the velocity of the *diffractive pattern* at the location of the Earth, is estimated from the decorrelation bandwidth ( $\Delta\nu$ ) and the diffractive scintillation time scale ( $T_{\text{diff}}$ ). Gupta et al. (1994) conclude that

$$V_{\text{iss}} = 3.85 \times 10^4 \sqrt{\frac{Dz \Delta\nu}{(1-z)}} \frac{1}{T_{\text{diff}} \nu_{\text{GHz}}} \text{ km s}^{-1} \quad (3)$$

where  $\nu_{\text{GHz}}$  is the observing frequency in GHz,  $D$  is in kpc,  $\Delta\nu$  is in MHz, and  $T_{\text{diff}}$  is in seconds. The variable  $z$  gives the fractional distance to the scattering screen, where  $z = 0$  gives the observer’s position, and  $z = 1$  gives the pulsar’s position. The value of decorrelation bandwidth is computed by the relation  $\Delta\nu = 1/(2\pi\tau_{\text{sc}})$ . When the effective scattering screen is midway along the LOS ( $z = 0.5$ ),  $V_{\text{iss}} = V_p$ , and when the screen is at the location of the pulsar ( $z = 1.0$ ),  $V_{\text{iss}} = \infty$ . While doing this, an important assumption is that the pulsar proper motion is dominant over contributions from differential Galactic motion, solar peculiar velocity, and the Earth’s annual orbital modulation. In the case of PSR B1937+21, this assumption is not justified. The effective scattering screen, which is located somewhere along the LOS, has a Galactic motion whose component along the LOS direction is different from that of the pulsar or the Sun. In order to correct for this effect, let us calculate the LOS velocity across the effective scattering screen at a fractional distance  $z$  from the observer:

$$V_\perp = 3.85 \times 10^4 \frac{\sqrt{Dz(1-z)\Delta\nu}}{T_{\text{diff}} \nu_{\text{GHz}}} \text{ km s}^{-1} \quad (4)$$

Then, let us assume that the scattering along the LOS can be adequately expressed by having a thin screen alone, at a

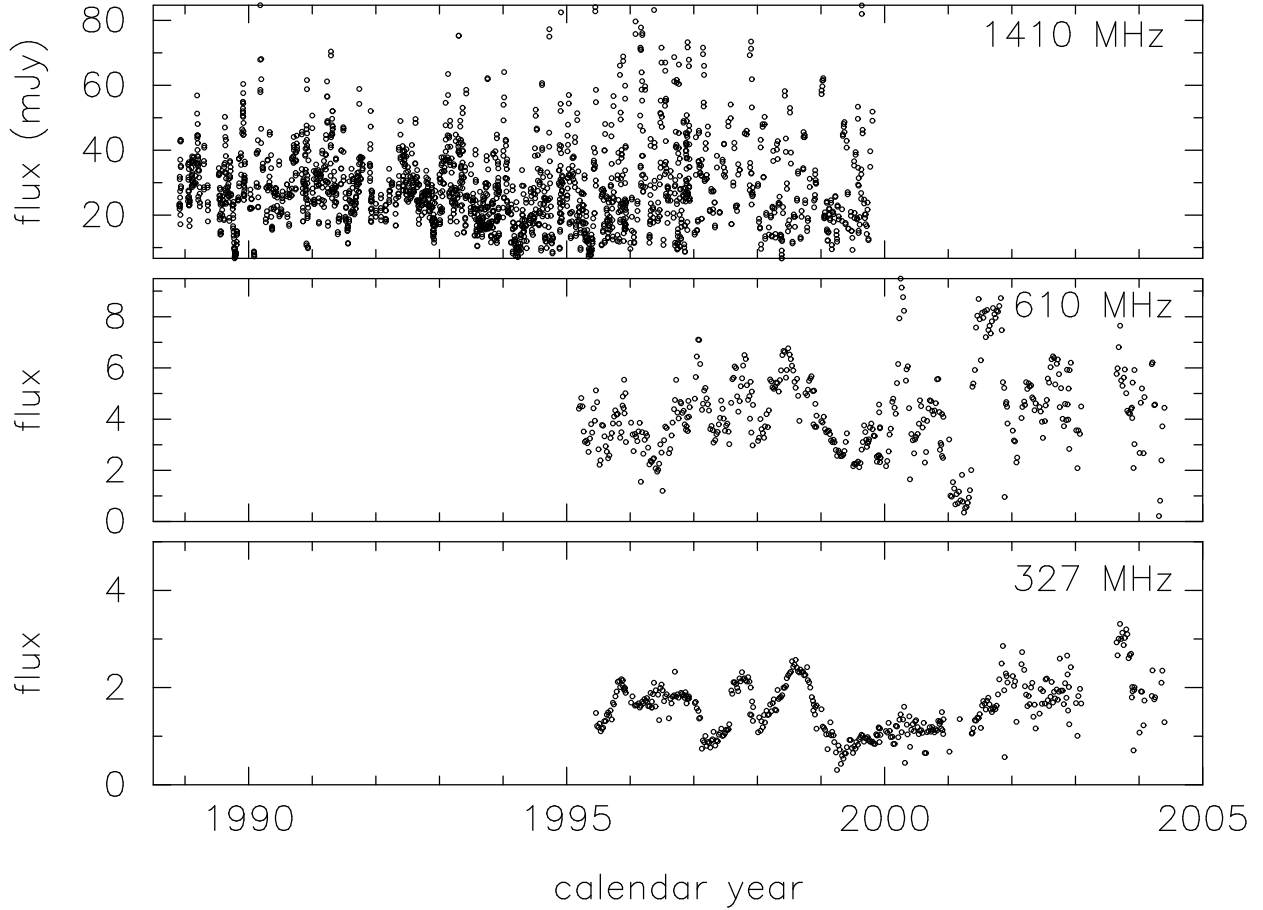


FIG. 3.— Measured flux density as a function of time. The top panel corresponds to the radio frequency of 1410 MHz with the data obtained from Nançay telescope, the middle and the bottom panel to 610 and 327 MHz with the data obtained from the Green Bank 85-ft telescope.

distance of  $D_s = zD$  from the observer. Then, Equation 2 can be expressed as

$$\tau_{\text{sc}} = \frac{\psi_0}{2c} D z (1-z) \quad (5)$$

$$\theta_H^2 = 4 \ln 2 (1-z)^2 \psi_0 \quad (6)$$

Here,  $\psi_0$  gives the mean scattering rate corresponding to the effective thin screen. Then, let us express independently the transverse velocity of the LOS across the scattering screen as

$$\begin{aligned} \vec{V}'_{\perp} &= (1-z)\vec{V}_e + z\vec{V}_p - \vec{V}_G(zD\hat{n}) \\ &= \vec{V}_e + zD\vec{\mu} - \vec{V}_G(zD\hat{n}), \end{aligned} \quad (7)$$

where  $V_e$  is Earth's orbital velocity,  $V_p$  is the pulsar transverse velocity in its LSR, and  $V_G$  is the transverse velocity contribution from the Galactic differential motion to the screen.  $V_E$  gives the contribution of the Earth's motion on the LOS velocity across the screen.

Equations 4 and 7 give two independent estimates of the line of sight velocity across the effective scattering screen and therefore allow us to solve for the value of  $z$  given  $D$ . With  $D = 3.6$  kpc (Cordes & Lazio 2002), we find  $z = 0.7$ . The LOS velocity is  $51 \text{ km s}^{-1}$ . The assumed value of  $T_{\text{diff}}$  is 78 seconds at 327 MHz (scaled from 444 seconds at 1400 MHz of Cordes et al. 1991), and the value of  $\Delta\nu$  is 0.0013 MHz calculated from  $\tau_{\text{sc}} = 120 \mu\text{s}$ .

To summarize, the measured value of  $\theta_H = 14.6 \pm 1.8$  mas and the estimated value of  $\theta_{\tau}$  are consistent with each other,

suggesting a uniformly distributed scattering medium. On the other hand, comparison of velocity components,  $V_p$ ,  $V_{\perp}$  and  $V'_{\text{los}}$  suggest a thin-screen at  $z \sim 2/3$ . As Deshpande & Ramachandran (1998) demonstrate, this solution is equivalent to having a uniformly distributed scattering medium! Therefore, we conclude that the line of sight to PSR B1937+21 can be described adequately by a uniformly distributed scattering matter.

The Earth's orbital velocity around the Sun will modulate the observed scintillation speed, and therefore the diffractive scintillation time scale, with a one-year time scale. The amplitude of this modulation will depend on the effective  $z$  of the diffracting material, and so monitoring could provide an estimate of the effective screen location. If the effective screen is close to the Earth, then the modulation is strong, and if it is located close to the pulsar, then it is negligible. Figure 5 demonstrates this effect. The ordinate and abscissa give the LOS velocity across the effective scattering screen along the galactic longitude and latitude, respectively. For an assumed distance of 3.6 kpc, the straight line shows the expected centroid velocity of  $V'_{\perp}$ . The left most end of the line (origin of the plot) corresponds to  $z = 0$ , and the right most end corresponds to  $z = 1$ . The annual modulation of  $V'_{\perp}$ , shown as the two ellipses, correspond to  $z=0.5$  and  $z = 2/3$ . We have no way of identifying this annual modulation in our data, as we are insensitive to diffractive effects in our data set.

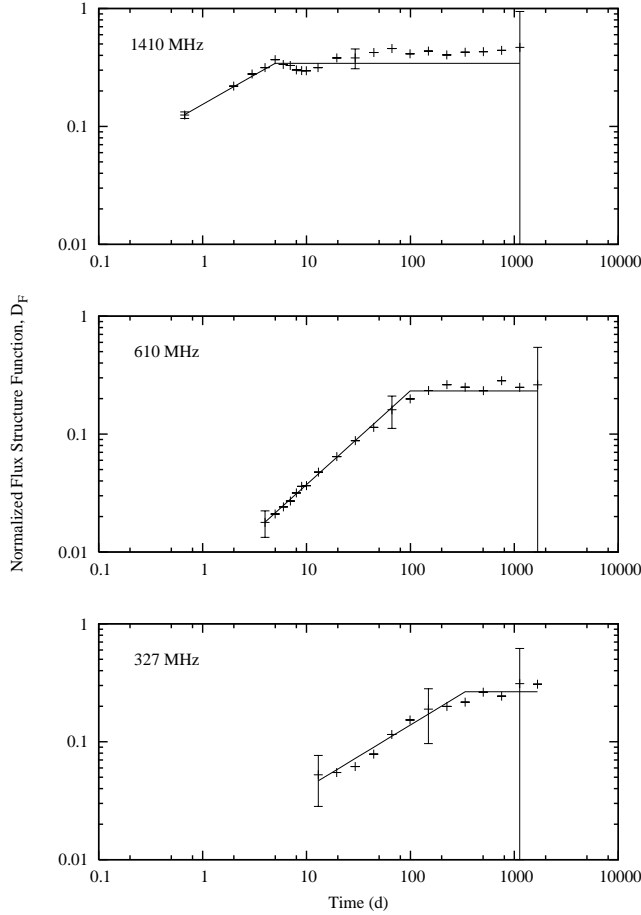


FIG. 4.— Structure function of normalized flux variations at 1410 MHz (Top), 610 MHz (middle), and 327 MHz (bottom). The 1410 MHz data was obtained from Nançay telescope. The saturation value of the structure function at larger lag values indicates the observed modulation index. Error bars are shown on only a few points, to preserve clarity. See text for details.

Another measurement that could help us is the direct measurement of distance to this object by parallax measurements. Chatterjee et al. (2005, private communication), from their preliminary Very Long Baseline Array (VLBA) based parallax measurements, report that the distance to PSR B1937+21 is  $2.3_{-0.5}^{+0.8}$  kpc, if they force the proper motion value to be the same as that of our timing based measurements (Table 2). In the coming year, accuracy of their measurements will improve with further sensitive observations.

## 5. REFRACTIVE SCINTILLATION

### 5.1. Parameter estimation

We determine refractive scintillation parameters from the data presented in Figure 3 following the structure function approach in previous studies (Stinebring et al 2000; Kaspi & Stinebring; Rickett & Lyne 1990). We define the structure function  $D_F$  for flux time series  $F(t)$  as

$$D_F(\delta t) = \frac{\langle [F(t) - F(t + \delta t)]^2 \rangle}{\langle F(t) \rangle^2}, \quad (8)$$

where  $\delta t$  is a time delay. Since our flux measurements occur at discrete and unevenly spaced time intervals, we compute the flux difference for all possible lags, then average results into logarithmically spaced bins.

The flux structure function typically has a form described by Kaspi & Stinebring et al. (1992) - a flat, noise dominated section at small lags, then a power-law increase which finally saturates at a value  $D_s$  at large lags. In practice, the saturation regime may have large ripples in it, an effect of the finite length of any data set. In addition, the measured flux structure function is offset from the “true” flux structure function due to a contribution from uncorrelated measurement errors. At 327 MHz and 610 MHz, we estimate this noise term from the short-lag (noise regime) values. At 1410 MHz (from Nançay), we use the individual flux error bars to get the noise level. After subtracting the noise value, we fit the result to a function of the form

$$D_F(\delta t) = \begin{cases} D_s(\delta t/T_s)^\alpha, & [0 < \delta t < T_s] \\ D_s, & [\delta t > T_s] \end{cases} \quad (9)$$

In this fit, the power law slope  $\alpha$ , the saturation timescale  $T_s$ , and the saturation value  $D_s$  are all free parameters. The flux structure function data and fits are shown in Figure 4.

As shown in Rickett & Lyne (1990), the refractive parameters can be measured from the flux structure function using the following relationships: The modulation index  $m$  is given by  $m = \sqrt{D_s/2}$ , and the refractive scintillation timescale  $T_{\text{ref}}$  is given by  $D_F(T_{\text{ref}}) = D_s/2$ . All the measured parameters, including those measured by earlier investigators are summarized in Table 3.

Based on a propagation model through a simple power-law density fluctuation spectrum, we expect to see refractive variations in the flux measurements on a timescale  $T_{\text{ref}} \sim 0.5\theta_H D/V_\perp$ , where  $V_\perp$  is the line of sight velocity across the effective scattering screen. For the argument sake, if we assume an effective scattering screen at  $z = 0.5$ , then  $V_\perp \sim 40 \text{ km sec}^{-1}$ . With  $\theta_H = 14.6 \text{ mas}$ , the expected refractive scintillation time scale is  $\sim 3$  years at 327 MHz. This is more than an order of magnitude in excess of the measured value. Furthermore, if the density fluctuations in the medium are distributed according to the Kolmogorov power law distribution, then the expected frequency scaling law is  $T_{\text{ref}} \propto \lambda^{2.2}$ . Our measured values indicate a significantly different scaling. Although it is consistent with  $T_{\text{ref}} \propto \lambda^{2.2}$  between 610 and 1420 MHz, it is not so between 327 and 610 MHz, where it is consistent with being directly proportional to  $\lambda$ . Our observed modulation index ( $m$ ) values are also considerably larger than predicted, and show a “flatter” wavelength dependence, as listed in Table 3. We will address this issue in detail in the following section.

### 5.2. Nature of the spectrum – inner scale cutoff

The three disagreements with a simple model summarized in §5.1 force us to explore a few aspects of the electron density power spectrum that may possibly explain what we observe. The effects of *caustics* on the observed scintillations have been explored by several earlier investigators, most notably Goodman et al. (1987) and Blandford & Narayan (1985). In particular, if the power law scale distribution in the medium is truncated at an inner scale that is considerably larger than the diffractive scale, as they show, the observed flux variations are dominated by caustics. This is of great interest to us, as this seems to explain all the discrepancies that we note in our observed refractive parameters. For instance, as Goodman et

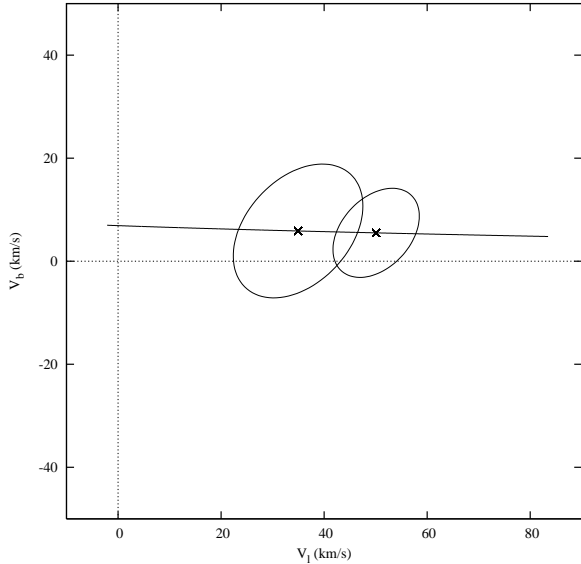


FIG. 5.— Estimated line of sight transverse velocity across the effective scattering screen at a distance of  $zD$  from the Sun. The velocity is resolved into the components along galactic longitude ( $V_l$ ) and latitude ( $V_b$ ). We have assumed a distance of 3.6 kpc to the pulsar from the Sun. Any point on the line indicates a combination of  $V_l$  and  $V_b$  corresponding to a value of  $z$ , with the left most end for  $z = 0$  and the right most end for  $z = 1$ . The line itself does not include the Earth’s orbital velocity contribution. The annual modulation due to Earth’s motion in its orbit is shown as the ellipses. The two ellipses correspond to the scenarios of  $z = 0.5$  and  $z = 2/3$ .

al. (1987) show that if the inner scale cutoff is a considerable fraction of the Fresnel scale, then the observed fluctuation spectrum of flux is dominated by fluctuation frequencies that are lower than the diffractive frequencies, but significantly higher than that expected from refractive scintillation. This is what we observe. Moreover, as they note, the observed wavelength dependence of the refractive time scale, as well as the modulation index is expected to be “shallower” than the expected values of  $\lambda^{2.2}$  and  $\lambda^{-0.57}$ , respectively.

A “shallow” frequency dependence of the modulation index has been reported by others (Coles et al. 1987; Kaspi & Stinebring 1992; Gupta et al. 1993; Stinebring et al. 2000). While Kaspi & Stinebring (1992) find that the observed refractive quantities matched well with the predicted values for five objects, three other objects, especially PSR B0833–45, has a significantly shorter measured  $T_{\text{ref}}$  and greater modulation index than expected. This is very similar to our situation here with PSR B1937+21.

Stinebring et al. (2000) concluded that the 21 objects that they analysed fell into two groups. The first group followed the frequency dependence predicted by a Kolmogorov spectrum with the inner cutoff scale far less than the diffractive scales (*Kolmogorov-consistent group*). The second group, which is the *super-Kolmogorov group*, is consistent with a Kolmogorov spectrum with an inner scale cutoff at  $\sim 10^8$  meters. The observed modulation indices were consistently greater than that of the Kolmogorov predictions, as we have seen in our measurements of PSR B1937+21. This group includes pulsars like PSRs B0833–45 (Vela), B0531+21 (Crab), B0835–41, B1911–04 and B1933+16. An important physical property that binds them all is that, excepting one object, all

objects have a strong *thin-screen* scatterer somewhere along the LOS. This is either a supernova remnant (or a plerion) like in the case of Vela and Crab pulsars, a HII region as in the case of B1942–03 and B1642–03, or a Wolf-Reyet star as in the case of B1933+16 (see Prentice & ter Haar 1969; Smith 1968). Although our measurements show that pulsar PSR B1937+21 is consistent with the characteristics of the *super-Kolmogorov* group, as we describe in §4, we find no compelling evidence for the presence of any dominant scatterer somewhere along the LOS.

To summarize, while some investigators have reported agreement of the measured refractive properties with the theoretical expectations from a Kolmogorov spectrum with an infinitesimally small inner scale, there are a considerable number of cases where the observed properties are significantly different from that predicted by the simple Kolmogorov spectrum. These other cases can be explained by invoking spectrum with a large inner scale cutoff, including the case where the cutoff approaches the Fresnel radius and leads to a caustic-dominated regime. From Gupta et al. (1993) and Stinebring et al. (2000), the modulation index can be specified as a function of the inner cutoff scale as

$$m = 0.85 \left( \frac{\Delta\nu}{\nu} \right)^{0.108} \left( \frac{r_i}{10^8 \text{m}} \right)^{0.167} D_{\text{kpc}}^{-0.0294}. \quad (10)$$

With the known value of  $\Delta\nu$  at 327 MHz of 1.33 kHz, the distance to the pulsar of 3.6 kpc, and the observed modulation index of 0.39, the inner scale cutoff,  $r_i$ , comes to  $1.3 \times 10^9$  meters.

## 6. DM VARIATIONS

We turn now to the dispersion measure variations presented in Figure 6 that sample density variations on transverse scales much larger than those involved with diffractive and refractive effects. The most striking feature in Figure 6 is the large secular decline from  $71.040 \text{ pc cm}^{-3}$  in 1985 to  $71.033 \text{ pc cm}^{-3}$  in 1991 and then to  $71.022 \text{ pc cm}^{-3}$  by late 2004. These long-term secular variations are many times greater than the RMS fluctuations of  $\sim 10^{-3} \text{ pc cm}^{-3}$  on short time scales. An important question that arises is whether these variations are the result of a spectrum of electron-density turbulence, or whether there might be a contribution from the smooth gradient of a cloud, or clouds along the LOS. We look at this question from two angles. First we present a phase structure function analysis of the dispersion measure data and estimate a power-law index of the electron density spectrum. Then we estimate the probability that such a spectrum would produce a 22-y realization that was so strongly dominated by the large, monotonic changes mentioned above.

We write the power spectrum of electron-density fluctuations as

$$P(q) = C_n^2 q^{-\beta}, \quad [q_o < q < q_i] \quad (11)$$

where  $\beta$  is the power law index,  $q_o$  and  $q_i$  are the spatial frequencies corresponding to the outer and the inner boundary scale, within which this power law description is valid.  $C_n^2$  is the amplitude, or strength, of the fluctuations. A quantity that is closely related to the density spectrum which can be quantified by observable variables is the phase structure function,  $D_\phi(b)$ , with  $b = 2\pi/q$ . This is defined as the mean square geometric phase between two straight line paths to the observer, with a separating distance of  $b$  between them in the plane normal to the observer’s sight line. The phase structure function and the density power spectrum are related by a transform

TABLE 3  
MEASURED AND EXPECTED PARAMETERS.

$\tau_{sc}$ ( $\mu$ s)	$\theta_H$ (mas)	$T_{diff}$ (s)	$T_{ref}$		$m$		$\nu$ (MHz)
			observed	expected	observed	expected	
120 <sup>†</sup>	14.6 <sup>b</sup>	–	73 days	3 y <sup>f</sup>	0.33	0.14 <sup>c</sup>	327
38 <sup>e</sup>	–	100 <sup>e</sup>	–	–	–	–	430
–	–	–	43.9 days	6 mon <sup>g</sup>	0.39	0.2	610
–	–	260 <sup>a</sup>	3 days <sup>d</sup>	45 days <sup>g</sup>	0.45	0.33 <sup>c</sup>	1400
0.17 <sup>e</sup>	–	444 <sup>e</sup>	–	–	–	–	1400

<sup>†</sup> Has a time dependent RMS variation of 20 $\mu$ s

<sup>a</sup> Cordes et al. (1986)

<sup>b</sup> Gwinn et al. (1993)

<sup>c</sup> Romani et al. (1986); Kaspi & Stinebring (1992)

<sup>d</sup> Lestrade et al. (1998) give the value as 13 days

<sup>e</sup> Cordes et al. 1990

<sup>f</sup> Calculated with  $T_{ref} \sim \theta_H D / 2V_{\perp}$

<sup>g</sup> Extrapolated with  $T_{ref} \propto \lambda^{2.2}$

(Rickett 1990; Armstrong, Rickett, Spangler 1995),

$$D_{\phi}(b) = \int_0^{\infty} 8\pi^2 \lambda^2 r_e^2 dz' \int_0^{\infty} q [1 - J_0(bqz'/z)] dq \times P(q=0) \quad (12)$$

Here,  $r_e$  is the classical electron radius ( $2.82 \times 10^{-15}$  meters),  $J_0$  is the Bessel function. Under the conditions that we have assumed,  $D_{\phi}(b)$  is also a power law (Rickett 1990; Armstrong, Rickett & Spangler 1995), given by

$$D_{\phi}(b) = \left( \frac{b}{b_{coh}} \right)^{\beta-2} \quad (13)$$

where  $b_{coh}$  is the coherence spatial scale. Dispersion measure can be written as

$$DM = 2.410 \times 10^{-16} \left[ \frac{(\nu_1^2 - \nu_2^2)}{\nu_1^2 \nu_2^2} \right] \left( \frac{\Delta\phi}{f} \right) \text{ pc cm}^{-3}, \quad (14)$$

where  $\Delta\phi$  is the difference in the arrival phases ( $\phi_2 - \phi_1$ ) of the pulse at the two barycentric radio frequencies (Hz)  $\nu_1$  and  $\nu_2$ , with  $f$  being the barycentric rotation frequency (Hz) of the pulsar. With this linear relation between DM and geometric phase difference, then structure function can be written as (KTR94)

$$D_{\phi}(b_o) = \left( \frac{2\pi}{\nu} \frac{\text{Hz}}{2.410 \times 10^{-16} \text{ pc cm}^{-3}} \right)^2 \times \langle [DM(b+b_o) - DM(b)]^2 \rangle. \quad (15)$$

Here, the angular brackets indicate ensemble averaging. The transformation between the spatial coordinate  $b$  (and the spatial delay  $b_o$ ) and the time coordinate  $t$  (or time delay  $\tau$ ) is simply given by  $b = V_{\perp} t$ , where  $V_{\perp}$  is the transverse velocity of the LOS across the effective scattering screen.

With the understanding that any difference in DM that we compute for a time baseline from Figure 6 corresponds to a point in the phase structure function, we can derive the phase structure function on the basis of Equation 15. This is given in Figure 7.

There are several important points in Figure 7. The solid line gives the best fit line for the data in the time interval of 5 days to 2000 days. The derived values of the intercept and the power law index ( $\beta$ ) are,

$$\begin{aligned} \text{intercept} &= 4.46 \pm 0.09 \\ \beta &= 3.66 \pm 0.04 \end{aligned} \quad (16)$$

The value of  $\beta$  is remarkably close to the value expected from a Kolmogorov power law distribution ( $\beta = 11/3$ ). We are using the terminology ‘‘intercept’’ only to indicate the value of  $\log[D_{\phi}(\tau)]$  when  $\log[\text{timelag}(\text{days})]$  is zero. Here, a cautionary remark is warranted. Given the finite time span of our data set, and the fact that the low spatial frequencies dominate the long term variations in DM, we do not have a stationary sample of noise spectrum. We have estimated the error in each bin of the structure function as

$$\sigma_s = \frac{\sigma_D}{\sqrt{N_i}},$$

where  $\sigma_D$  is the root mean square deviation with respect to the mean phase structure function value in a bin,  $D_{\phi}(\tau)$ , and  $N_i$  is the number of ‘‘independent’’ samples in the bin. This is estimated as the smaller of  $(T/\tau)$  and the actual number of samples that have gone into the estimation of  $D_{\phi}(\tau)$ . Here,  $T$  is the time span of the data.

By assuming that the transverse speed of the sightline across the effective scattering screen is  $\sim 40 \text{ km sec}^{-1}$  (half of pulsar’s velocity in its LSR), we can translate the delay range between which this slope is valid, to 0.2 to 50 A.U.

The time delay value corresponding to the phase structure function value of unity is, by definition, the coherent diffractive time scale ( $T_{diff}$ ) at the corresponding radio frequency, with the assumption that the scattering material is uniformly distributed along the LOS. From the fit parameters given in Equation 16, this delay is 180 seconds. This should be compared with the measured  $T_{diff}$  value of  $444 \pm 28$  seconds tabulated in Table 3. If we interpret the inner scale cutoff value of  $r_i \sim 1.3 \times 10^9$  meters as the scale size below which the slope ( $\beta$ ) of the density fluctuation spectrum changes to a value greater than that given in Equation 16, then the fact that the measured  $T_{diff}$  value of 444 seconds being significantly greater than 180 seconds is understandable. In the limiting case, where the slope of the density irregularity power spectrum changes to the critical value of  $\beta = 4$  below the inner scale cutoff value, the expected  $T_{diff}$  value is about 1100 seconds. This makes it very important to measure the exact frequency dependence of the diffractive parameters like temporal scatter broadening and diffractive scintillation time scale. To the best of our knowledge, Cordes et al. (1990) show the most complete multi-frequency measurements of the diffractive scintillation parameters of this pulsars. Their measurements are not accurate enough to distinguish between such small variations in slope.

While our analysis of DM variability suggests a Kolmogorov spectrum at AU scales, we are struck by the long term monotonic decrease of DM and wonder if we might be seeing the effects of smooth gradients in large scale galactic structures that are not part of a turbulent cascade. We performed a Monte Carlo simulation to investigate this. In each realization of the simulation, we generated with a different random number seed, a screen of density fluctuations. We assumed that the random fluctuations corresponding to a given spatial frequency are described by a Gaussian function, but the total power as a function of spatial frequencies is described by a single power law of index  $-11/3$ . Assuming that the screen is located at the mid point along the sight line, we let the pulsar drift with its transverse velocity, and measured the implied column density (DM) as a function of time.

We developed a procedure similar to that of Deshpande (2000) to compare the observed  $DM(t)$  curve with the simulated ones. From the observed  $DM(t)$  curve, we computed the



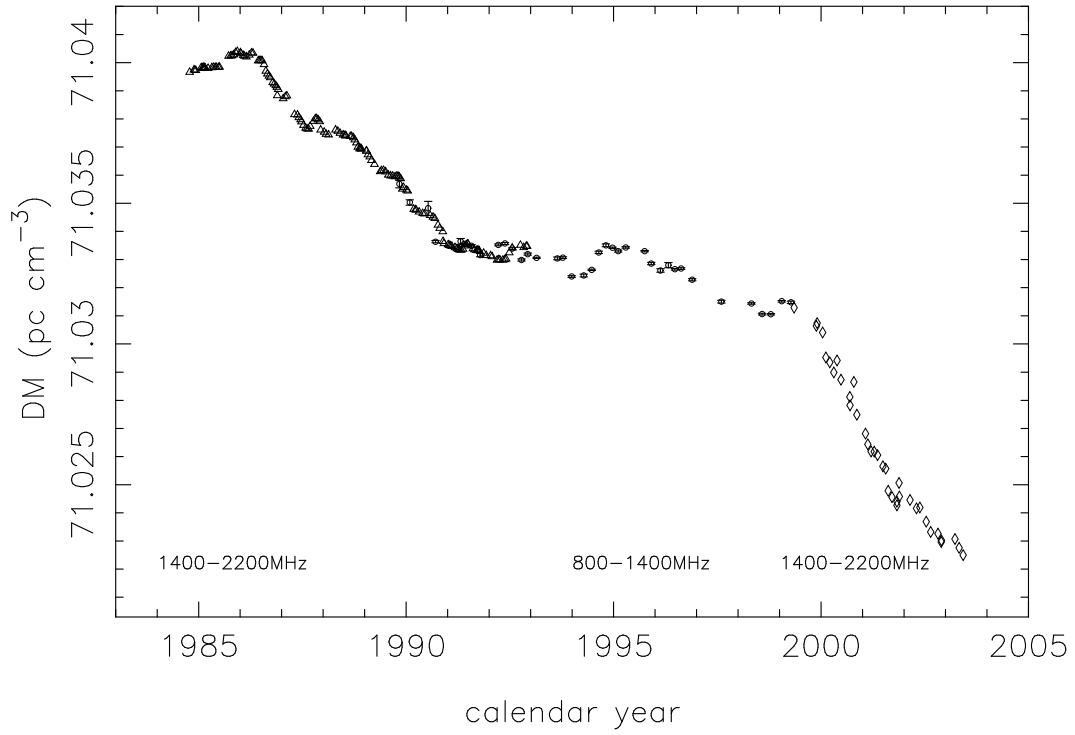


FIG. 6.— Dispersion Measure as a function of time. Open triangles give the measurements of KTR94 at 1400 and 2200 MHz, open circles are from our Green Bank 140-ft telescope measurements at 800 and 1400 MHz, and the open diamond symbols indicate our measurements from the Arecibo Observatory, at 1420 and 2200 MHz. All error bars indicate RMS errors.

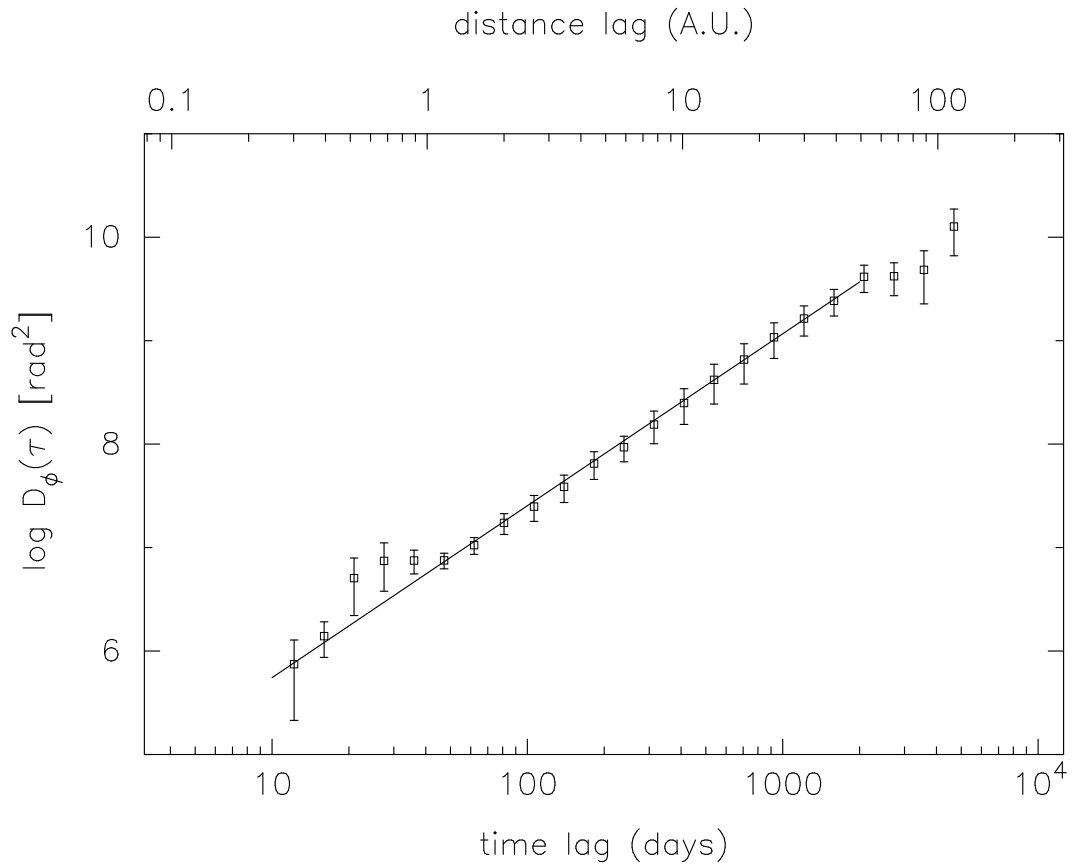


FIG. 7.— The phase structure function derived with the help of Equation 15 from the data displayed in Figure 6. Solid line represents the best fit for the data in the time range of 30 days to 2000 days. For translating the time delay range into a space delay, we have assumed a sightline transverse velocity of  $40 \text{ km sec}^{-1}$ , which is half of the pulsar's peculiar velocity in its LSR. We have assumed an effective screen at a fractional distance of 0.5. See text for details.

parameter  $\Delta DM = [DM(t) - DM(t - \tau_c)]$ , where  $\tau_c$  is the time delay. Our aim is to compare the distribution of this parameter in very short delays and very large delays. As we can see in Figure 7, the structure function describes a well defined slope between the delay range of  $\sim 30$  days to  $\sim 2000$  days. We defined two delay bins, 30–60 and 1300–2000 days, within which we monitored the distribution function of the quantity  $\Delta DM$ . From this, we could infer that the distribution at the bin of 1300–2000 days had a span of  $\sim 20\sigma_s$ , where  $\sigma_s$  is the RMS deviation of the distribution at the delay range of 30–60 days. That is, the  $\Delta DM$  values that we see at largest delays is as high as 20 times that of the typical deviations at short delays. We performed the same procedure on the simulated set of data to quantify the likelihood of such deviations. We simulated 1024 number phase screens. Out of these 1024 screens, we found that such large deviations were possible  $\sim 7\%$  of the times. This is perhaps not surprising, as with such a steep spectrum, it is obvious that most of the power is in large scales (smaller spatial frequencies), and hence they tend to dominate our  $\Delta DM$  measurements. We conclude that while monotonic changes of this magnitude are rare, it is consistent with a turbulent cascade spectrum of density fluctuations.

#### 7. FREQUENCY DEPENDENCE OF DM

Dispersion depends on the column density of electrons. In a uniform medium radio wave propagation senses the average density in a tube whose beam waist is set by the Fresnel radius  $\sqrt{z(1-z)\lambda D}$ . In a turbulent medium frequency-dependent multipath propagation can expand this tube considerably. With refraction, the center of the tube wanders from the geometric LOS. Indeed there may be a number of wave propagation tubes, each with their independent relative gain. The consequence is that DM and related effects will show frequency dependence:

1. the effective DM depends on frequency.
2. the DM variations at lower frequencies will be much “smoother” than that at higher frequencies, as the apparent angular size of the source acts as a *smoothing function* on the measured DM variations.
3. since the apparent size of the source is larger at low frequencies, some features of the ISM that are visible at lower frequencies may be invisible at higher frequencies!

We can explore these effects by assuming that the timing residuals at 327 MHz and 610 MHz, which are relative to the timing model derived at higher frequencies that included removal of DM variations, are due to DM variations. The smoothing effect of scattering could be revealed by a spectral analysis. The slow variations were removed to pre-whiten the spectrum that would otherwise be severely contaminated. The 327 MHz data was fit to a fourth order polynomial and the result was subtracted from both data sets. The two right side panels give the residual DM values after subtracting the best fit curve from the actual DM curve. The resulting spectral comparison fails to have sufficient signal to clearly demonstrate increased smoothing at 327 MHz relative to 610 MHz. Higher signal-to-noise ratio is required. The DM variations relative to long term trends in the right-hand panels of Figure 8 are different.

An important source of systematic error that can affect our analysis here is the effect of scattering on the derived DM as

a function of time at a given frequency. At 327 MHz, as we described in §3, we perform an elaborate procedure to fit for the scatter broadening of the pulse profile, in order to compute the “true” TOA of the profile. However, we do not follow this procedure at 610 MHz (or any other higher frequency). The error due to this can be quantified easily from Figure 2. The temporal scatter broadening value varies by an RMS value of some  $19.6 \mu\text{s}$ . With the wavelength dependence of  $\tau_{\text{sc}} \propto \lambda^{4.4}$ , the expected RMS variation at 610 MHz is  $1.3 \mu\text{s}$ . The equivalent DM perturbation at 610 MHz with respect to infinite frequency is  $\sim 10^{-4} \text{ pc cm}^{-3}$ .

#### 8. ACHIEVABLE TIMING ACCURACY

In this section, we will estimate quantitatively errors introduced by various scintillation related effects. For PSR B1937+21, although a typical observation with highly sensitive telescopes like Arecibo telescope helps us achieve a TOA accuracy of a few tens of nanoseconds, the ultimate long term accuracy seems to be far greater than this. In general, it is a combination of frequency independent “intrinsic timing noise” from the pulsar itself, and the frequency dependent effects, such as what we are addressing here. With some 18 years of data at 800, 1400 and 2200 MHz, Lommen (2002) quantifies the timing timing residual, after fitting for position, proper motion, rotation frequency and its time derivative (see also Kaspi et al. 1994). A large fraction of the left over residuals is presumably the intrinsic timing noise. As we have mentioned before, we have absorbed a good part of this by fitting for the second time derivative of the rotation frequency,  $\ddot{f}$  (see Table 2). In this section, our aim is to quantify possible timing errors from various “chromatic” effects related to interstellar scintillation.

##### 8.1. Fluctuation of apparent angular size

The temporal variability of pulse broadening,  $\tau_{\text{sc}}$ , (as shown in Figure 2) means that even the apparent angular broadening of the source,  $\theta_H$ , is also changing as a function of time. Since  $\tau_{\text{sc}} \propto \theta_H^2$ , with the RMS variation in  $\tau_{\text{sc}}$  of  $19.6 \mu\text{s}$  at the radio frequency of 327 MHz, the corresponding variation in  $\theta_H$  comes out to be  $\sim 8\%$  of the mean value. This change occurs with typical time scales of  $\sim 67$  days, which is the time scale with which  $\tau_{\text{sc}}$  changes. Since we have only one epoch of  $\theta_H$  measurement, we have no way of observationally verifying the mean value or the time scale of its variation.

##### 8.2. Image wandering and the associated timing error

Due to non-diffractive scintillation that “steers” the direction of rays (“refractive focussing”), the position of the pulsar is expected to change as a function of time. This is an important and significant effect, as it introduces a TOA residual as a function of time, depending on the instantaneous position of source on the sky. Several authors have investigated this effect in the past (Cordes et al. 1986; Romani et al. 1986; Rickett & Coles 1988; Fey & Mutel 93; Lazio & Fey 2001). For a Kolmogorov spectrum of irregularities ( $\beta = 11/3$ ) with infinitesimally small inner scale cutoff, Cordes et al. (1986) predict the value of RMS image wandering as

$$\langle \delta\theta^2 \rangle^{1/2} = 0.18 \text{ mas} \left( \frac{D_{\text{kpc}}}{\lambda_{\text{cm}}} \right)^{-1/6} \theta_H^{2/3} \quad (17)$$

For an assumed distance to PSR B1937+21 of 3.6 kpc, this comes to 2 mas at 327 MHz (wavelength,  $\lambda = 92 \text{ cm}$ ). The

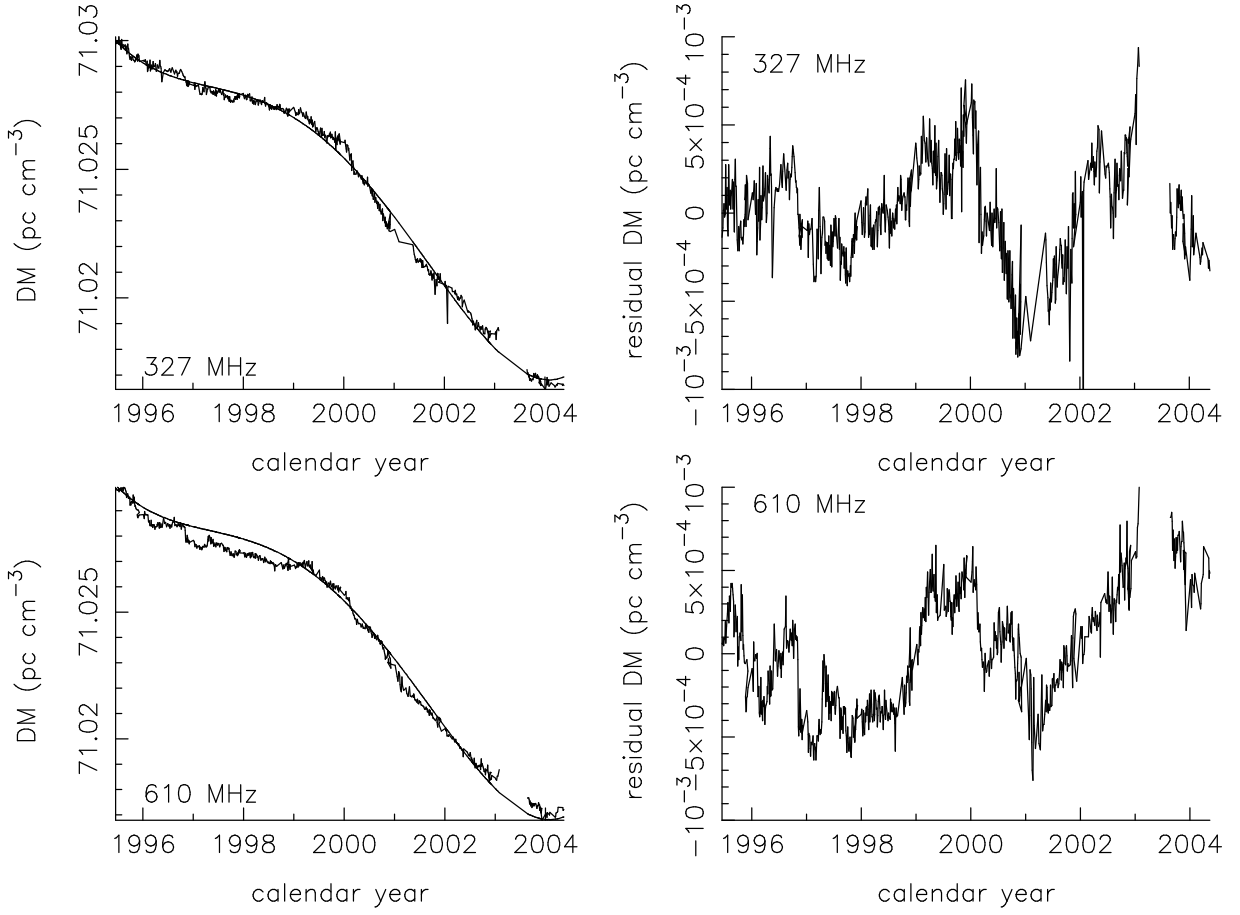


FIG. 8.— Dispersion Measure variations at 327 and 610 MHz. The two left hand side panels give DM as a function of time. The 327 MHz best fit line, produced by a fourth order polynomial fit, is given as a solid line in both 327 and 610 MHz plots. The residual DM, which is the difference between the actual DM and the best fit line, is given in the right hand side panels. See text for details.

value of 2 mas is still significantly less than the apparent angular size of the source, 14.6 mas, measured by Gwinn et al. (1993). However, for a spectrum with a steeper slope or with a significantly larger inner scale cutoff (as in our case), the value of  $\langle \delta\theta^2 \rangle^{1/2}$  is expected to be much larger, perhaps comparable to the value of  $\theta_H$ .

In order to estimate the timing errors introduced by this image wandering, we need an estimate of scattering measure ( $SM$ ) and  $C_n^2$  along the LOS to this pulsar. Following Cordes et al. (1991),

$$\begin{aligned}
 SM &= \int_0^D C_n^2(x) dx \\
 &= \left( \frac{\theta_H}{128 \text{ mas}} \right)^{5/3} \nu_{\text{GHz}}^{11/3} \\
 &= 292 \left( \frac{\tau_{\text{sc}}}{D_{\text{kpc}}} \right)^{5/6} \nu_{\text{GHz}}^{11/3}. \quad (18)
 \end{aligned}$$

Here,  $\tau_{\text{sc}}$  is specified in seconds.  $SM$  is specified in units of  $\text{kpc m}^{-20/3}$ . Assuming a distance of 3.6 kpc,  $\tau_{\text{sc}} = 120 \mu\text{s}$ ,  $\nu = 0.327 \text{ GHz}$ , the value of  $SM$  comes to  $\sim 8.8 \times 10^{-4} \text{ kpc m}^{-20/3}$ . Assuming that the scattering material is uniformly distributed along the LOS,  $C_n^2 \sim 2.4 \times 10^{-4} \text{ m}^{-20/3}$ .

Then, for a Kolmogorov spectrum, the RMS timing residual due to the image wandering can be written as (Cordes et al.

1986)

$$\sigma_{\delta t_{\text{ig}}} = 26.5 \text{ ns } \nu^{-49/15} D^{2/3} \left( \frac{C_n^2}{10^{-4} \text{ m}^{-20/3}} \right)^{4/5}. \quad (19)$$

With the computed value of  $C_n^2$  and a distance of 3.6 kpc, this amounts to  $4.8 \mu\text{s}$  at 327 MHz. Given the frequency dependence, this effect can be minimized by timing the pulsar at higher frequencies. For instance, at frequencies of 1 GHz and 2.2 GHz, this error translates to 125 and 2 nanosec, respectively. However, given the significantly large value of the inner scale cutoff, the RMS timing error that we have computed may well be a lower limit, and it is likely to be higher.

Given the fact that the exact source position due to this effect is unknown at any given time, it is very difficult to compensate for this effect.

### 8.3. Positional errors in solar system barycentric corrections

As we saw above, due to image wandering, the apparent position of the source wanders in the sky. This introduces yet another timing error. While translating the TOA at the observatory to the solar system barycenter, we assume a position which is away from the actual apparent position at the time of observation. This introduces an error, which can be quantified as (Foster & Cordes 1990)

$$\Delta t_{\text{bary}} = \frac{1}{c} (\vec{r}_e \cdot \hat{n}) (1-z) \Delta\theta_r(\lambda). \quad (20)$$

Here,  $c$  is the velocity of light, the dot product term gives the projected extra path length travelled by the ray due to Earth's annual cycle around the Sun, and  $\Delta\theta_r(\lambda)$  is the positional error due to image wandering. Of course, this term is a function of frequency, and hence the error accumulated is different at different frequencies.

At 327 MHz, with an RMS image wandering angle of 2 mas, for an object at the ecliptic plane,  $\Delta t_{\text{bary}} \sim 2 \mu\text{s}$ . For PSR B1937+21, this error amounts to  $\sim 0.8 \mu\text{s}$ . At frequencies 1 GHz and 2.2 GHz, this error translates to 85 and 17 nanosec, respectively.

#### 8.4. Timing error due to DM variation as a function of frequency

An important issue that arises due to the frequency dependent DM variation is the timing accuracy. Pulsars like PSR B1937+21 are known for the accuracy to which one can compute the pulse TOA. Given this, one wishes to eliminate any error that is incurred due to systematic effects like what we have here. Between 327 and 610 MHz (the two curves in Figure 8), the typical relative fluctuation of DM that we see is about  $5 \times 10^{-4} \text{ pc cm}^{-3}$ . As we discussed before, this is purely due to the fact that the effective interstellar column length sampled at one frequency is different from that at another frequency, due to the scatter broadening of the source. At 610 MHz, this relative DM fluctuation corresponds to some  $6 \mu\text{s}$  at 610 MHz. That is, at 610 MHz, typically an unaccounted residual of  $6 \mu\text{s}$  is incurred due to just effective DM errors. Even if the behavior of the pulse emission is extremely stable, at low frequencies, interstellar scattering limits our timing capabilities.

Due to the fact that dispersion delay goes as  $\nu^{-2}$ , although the above mentioned effect seems significant, one should be able to reduce it by going to higher frequencies. For instance, at 2.2 GHz, the DM-limited TOA error for PSR B1937+21 will be  $\sim 0.5 \mu\text{s}$ . This is not necessarily encouraging news, as a timing residual error of  $0.5 \mu\text{s}$  is large when compared to the accuracy that we can achieve in quantifying the TOAs (a few tens of ns) for this pulsar, given our observations with sensitive telescopes like Arecibo.

To summarize, although one takes into account time dependent DM changes while analysing the data, in order to achieve high accuracy timing, it is important to correct for a frequency dependent DM term. This introduces another dimension of correction in the timing analysis.

## 9. CONCLUDING REMARKS

We have presented in this paper a summary of over twenty years of timing of PSR B1937+21. These observations have been done over frequencies ranging from 327 MHz to 2.2 GHz with three different telescopes.

Given the agreement between the measured apparent angular broadening and that estimated by the temporal broadening, and the measured proper motion velocity and that estimated

by the knowledge of scintillation parameters, we conclude that the scattering material is uniformly distributed along the sightline.

There are three significant discrepancies between the expected values and the measured refractive parameters. These are,

1. The measured flux variation time scale is about an order of magnitude shorter than what is expected from the knowledge of the observed apparent angular broadening.
2. The flux variation time scale is observed to be directly proportional to the wavelength, whereas it is expected to vary as proportional to  $\lambda^{2.2}$  (for a Kolmogorov spectrum).
3. The flux modulation index is observed to have a wavelength dependence that is much "shallower" than the expected value.

These three discrepancies consistently imply that the optics is "caustic-dominated". This would mean that the density irregularity spectrum has a large inner scale cutoff,  $1.3 \times 10^9$  m. Our extrapolation of the phase structure function from the regime sampled by DM variations to the diffractive regime seems to indicate that the expected  $T_{\text{diff}}$  value is considerably shorter than the measured value. This is in favor of the above conclusion. Accurate measurements of frequency dependence of diffractive parameters is much needed.

In general, Millisecond pulsars are known for their timing stability. Potentially, we may achieve adequate accuracy in timing some of these pulsars to understand some of the most important questions related to the gravitational background radiation, or the internal structure of these neutron stars. However, our analysis here shows that interstellar scattering could be an important and significant source of timing error. As we have shown, although PSR B1937+21 is known to produce short term TOA errors as low as 10–20 nanosec with sensitive observations, the long term error is far larger than this. After fitting for  $\ddot{f}$  (which absorbs most of the achromatic timing noise), the best accuracy that we can achieve for this pulsar is  $0.9 \mu\text{sec}$  at 1.4 GHz, and about  $0.5 \mu\text{sec}$  at 2.2 GHz (by one of the authors, Andrea Lommen). It appears that almost all of this error can be accounted for by various effects that we have discussed in §8. In general, for millisecond pulsars with substantial DM, even if achromatic timing noise is small, interstellar medium may be a major source of timing noise.

We thank M. Kramer for sharing the data from the Effelsberg-Berkeley Pulsar Processor (EBPP), and S. Chatterjee and W. Brisken for sharing their VLBA based proper motion and parallax results of PSR B1937+21 prior to the publication. This work was in part supported by the NSF grant, AST-9820662.

## REFERENCES

- Armstrong, J.W., Rickett, B.J., Spangler, S.R. 1995, 443, 209  
 Backer, D.C., Hama, S., van Hook, S., Foster, R.S., 1993, ApJ, 404, 636  
 Backer, D.C., Wong, T., Valanju, J. 2000, ApJ, 543, 740  
 Blandford, R.D., & Narayan, R. 1985, MNRAS, 213, 591  
 Cognard, I., Bourgois, G., Lestrade, J.-F., et al. 1995, A&A, 296, 169  
 Coles, W.A., Frehlich, R.G., Rickett, B.J., Codona, J.L. 1987, ApJ, 315, 666  
 Cordes, J.M., Pidwerbetsky, A., & Lovelace, R.V.E. 1986, ApJ, 310, 737  
 Cordes, J. M., Wolszczan, A., Dewey, R. J., Blaskiewicz, M., Stinebring, D. R. 1990, ApJ, 349, 245  
 Cordes, J.M., Ryan, M., Weisberg, J. M., Frail, D. A., & Spangler, S. R. 1991, Nature, 354, 121  
 Cordes, J.M., & Rickett, B. J. 1998, ApJ, 507, 846  
 Cordes, J.M., & Lazio, T. J. W. 2002, astro-ph/0207156  
 Deshpande, A.A., & Ramachandran, R. 1998, MNRAS, 300, 577  
 Deshpande, A.A. 2000, MNRAS, 317, 199

- Fey, A.L., & Mutel, R.L. 1993, ApJ, 404, 197  
Foster, R.S., & Cordes, J.M. 1990, ApJ, 364, 123  
Foster, R.S., Fairhead, L., & Backer, D.C. 1991, ApJ, 378, 687  
Gupta, Y., Rickett, B.J., & Coles, W.A. 1993, ApJ, 403, 183  
Gwinn, C.R., Bartel, N., & Cordes, J.M. 1993, ApJ, 410, 673  
Kaspi, V.M., & Stinebring, D.R., 1992, ApJ, 392, 530  
Kaspi, V.M., Taylor, J.H., & Ryba, M.F. 1994, ApJ, 428, 713 (KTR94)  
Lazio, T.J.W., & Fey, A.L. 2001, ApJ, 560, 698  
Lestrade, J.-F., Rickett, B.J., & Cognard, I. 1998, A&A, 334, 1068  
Murray, C.A. 1986, Vectorial Astrometry, [Adam Hilger: Bristol]  
Phillips, J.A., & Wolszczan, A. 1991, ApJ, 382, L27  
Rankin, J.M., Comella, J.M., Craft, H.D., Jr. et al. 1970, ApJ, 162, 707  
Rankin, J.M., Counselman, C.C., III 1973, ApJ, 181, 875  
Rankin, J.M., & Isaacman, R. 1977 xx  
Prentice, A.J.R., ter Haar D. 1969, MNRAS, 146, 423  
Rickett, B.J., & Coles, W.A. 1988, in IAU Symp. 129, The Impact of VLBI  
on Astrophysics and Geophysics, ed. J. Moran & M. Reid (Dordrecht:  
Kluwer), 287  
Rickett, B.J. 1990, ARAA, 28, 561  
Rickett, B.J., & Lyne, A.G. 1990, MNRAS, 244, 68  
Smith, L. F. 1968, MNRAS, 141, 317  
Stinebring, D.R. et al. 1992, RScI, 63, 3551  
Stinebring, D.R., Smirnova, T.V., Hankins, T.H., et al. 2000, ApJ, 539, 300